Second Harmonic Super-resolution Microscopy for Quantification of mRNA at Single Copy Sensitivity

Jing Liu, Il-Hoon Cho, Yi Cui, and Joseph Irudayaraj*

Department of Agricultural and Biological Engineering, Bindley Bioscience Center, Birck Nanotechnology Center, Purdue University, West Lafayette, Indiana 47907, United States

ABSTRACT Cell-specific information on the quantity and localization of key mRNAs at single copy sensitivity in single cells is critical for evaluating basic cellular process, disease risk, and efficacy of therapy. Quantification of overexpressed mRNAs beyond the diffraction limit is constrained by the optical property of the probes and microscopy techniques. In this report, nanosized barium titanium oxide ($BaTiO_3$, BTO) crystals were utilized as probes for mRNA quantification by a second harmonic super-resolution microscopy (SHaSM). The SHaSM was able to detect a single copy of the human epidermal growth factor receptor 2 (Her2) mRNA at a resolution of 55.6 nm with the ability to resolve multiple mRNA copies in a diffraction-limited spot. Her2 mRNA per cell was counted in SK-BR-3, MCF-7, and HeLa cell lines as 595 ± 79.1, 38.9 ± 8.26, and 1.5 ± 2.8, respectively. Our single-cell quantification results were validated with the fluorescence *in situ* hybridization studies and quantitative PCR, showing better specificity and selectivity over current single-molecule approaches for transcript detection. The SHaSM is expected to have an upper limit of resolving ~10^4 transcripts in a single cell with the ability to monitor intracellular transcriptional dynamics at video rate. The developed approach has strong potential in clinical research and in the early diagnosis of life-threatening diseases such as cancer.

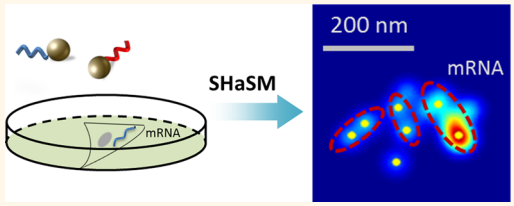

KEYWORDS: super-resolution microscopy · second harmonic generation · $BaTiO_3$ nanocrystals · single-copy detection · mRNA quantification · diagnostics

Far-field light microscopy is the most desirable approach to "visualize" the microscopic world inside a cell or live organisms for biological studies. The ubiquitous property of noninvasive detection has made it extraordinarily versatile for investigating fine structural details of the cellular architecture. In addition, the use of a fluorophore further enables the study of subcellular dynamics ranging from molecular interactions to intracellular events.

Despite the revolutionary significance, the conventional far-field light microscopy is restricted by the diffraction limit based on the scale diffraction theory;[1] that is, objects within a diffraction-limited spot, ~250 nm, cannot be resolved. However, many subcellular structures have features much smaller than this limitation, and numerous intracellular dynamics occur within this space.[2] Several approaches have been developed to break the diffraction barrier to achieve super-resolution. One such effort is to localize individual fluorescent probes to obtain subdiffraction resolution.[3−5] This stochastic super-resolution technique features two typical properties: the stochastic emission from single fluorescent molecules and the temporal modulation of the emission.[6] These two features can be realized by either repeated photoactivation or photoblinking of fluorescent molecules, such as fluorescent dyes, proteins, or quantum dots. However, these fluorescent probes can easily undergo photobleaching under tens or hundreds of activation cycles.[7] Quantum yield and photostability restrain the accuracy and applicability of this super-resolution technique.[7] In addition, the blinking of the quantum dots limits the application of imaging subcellular dynamics.[6] Furthermore, one-photon excitation configuration and total internal reflection imaging mode used in the stochastic super-resolution approaches constrain its application in deep-tissue imaging. These limitations demand the development of photostable probes and novel techniques for super-resolution imaging.

In this report, we demonstrate a novel second harmonic super-resolution microscopy

* Address correspondence to josephi@purdue.edu.

Received for review September 9, 2014 and accepted December 10, 2014.

Published online December 10, 2014
10.1021/nn505096t

(SHaSM), which was constructed on a scanning confocal microscopy platform taking advantage of ultrastable second harmonic generation (SHG) signals from nanosized crystals. Unlike the current super-resolution approaches which are based on fluorescent emission, the SHaSM collects ultrastable SHG emission from individual nanocrystals under the excitation of a two-photon laser source, overcoming the drawbacks of optical properties (photoblinking, photobleaching, quantum yield) and penetration depth of the fluorescence-based super-resolution imaging techniques.

SHG is a nonlinear optical process which converts two incident photons at a frequency ω into one photon at frequency 2ω.[8] This process only occurs in materials which lack inversion symmetry. Under the illumination of an ultrafast laser, the SHG material emits a transient, high-intensity, nonblinking, nonbleaching, unsaturated light pulse with an ultranarrow bandwidth (~5 nm).[9,10] Nanosized crystals, such as potassium titanyl phosphate ($KTiOPO_4$, KTP),[10−13] barium titanium oxide ($BaTiO_3$, BTO),[9,14,15] lithium niobate ($LiNbO_3$),[10−12] and lithium triborate (LiB_3O_5, LBO),[10−12] have been used to track molecular dynamics[16,17] and utilized for regular and holographic second harmonic imaging microscopy (SHIM)[14] and *in vivo* imaging.[9,18]

To demonstrate the applicability of SHaSM, the system design and the super-resolution features were applied to detect and quantify overexpressed transcripts at single-copy sensitivity. It has been established that variation in the transcription of key genes in single cells triggers the loss of tissue homeostasis.[19,20] Methods that can quantify the expression and localize the intracellular patterns of transcripts in single cells will pave the way for single-cell screening strategies that are rapid, quantitative, and clinically significant.[21] State-of-the-art techniques to detect mRNAs in single cells are based on fluorescence *in situ* hybridization (FISH),[22−28] in which fluorophore-labeled oligonucleotide probes[22,23] or fluorescent protein-tagged RNA binding protein (RBP) probes[24] were hybridized to the target transcript, making these visible as diffraction-limited fluorescence spots under conventional optical microscopy. However, the FISH approach failed to rigorously quantify overexpressed or nascent mRNA due to the diffraction-limited imaging tools and the optical flaws in the probes. In the FISH protocol, multiple fluorescence reporters were heavily labeled on a single oligonucleotide and multiple oligonucleotide probes were hybridized to a mRNA target to ensure detection sensitivity.[28−30] However, this approach sacrifices the fluorescence emission from individual dyes due to self-quenching or dye−dye interaction,[31] therefore making the intensity-scaled mRNA quantification at the single-copy limit questionable.[22]

In our work, we use BTO NCs as reporters for mRNA detection. Our strategy utilizes the concept of dimers formed from the hybridization of two BTO NC-conjugated probes targeting a mRNA in a sequence-specific manner. The dimer representing one single copy of mRNA will be resolved and quantified by the SHaSM with the spatial resolution of 55.6 nm, where it was possible to resolve and detect more than one mRNA in a single-diffraction-limited spot. This method can be applied to rigorously quantify the expression levels and the subcellular localization patterns of mRNAs at the sensitivity of a single copy, paving the pathway for quantitative monitoring of genetic information.

RESULTS AND DISCUSSION

The SHaSM is a stochastic super-resolution technique and shares two typical features with the localization-based super-resolution microscopies: (i) sufficient photons are generated from single particles and (ii) stochastic modulation of the emission is possible. Figure 1a shows the SHG emission from individual BTO NCs deposited on a coverslip, where more than 3000 photons could be collected within a dwell time of 0.6 ms at each pixel. More importantly, the SHG emission from single BTO NCs is polarization-dependent. SHG emission of the BTO NCs stems from the distortion of oxygen atoms in the tetragonal unit cell (Supporting Information (SI) section 1). Since the BTO crystal has the symmetry of class 4, the SHG emission is only determined by the *c*-axis of the unit cell (Figure S1).[8] Therefore, one can control the SHG emission by varying the angle between an incident electric field and the *c*-axis of the unit cell;[32] meanwhile, polarization response analysis of the SHG signal can report on the orientation of the unit cell,[33−35] which is beyond the scope of our study. Experimentally, we modulated the SHG signal from the BTO NCs by tuning the linear polarization angle of the excitation beam in the *ij* plane *via* a half-waveplate (SI section 1). Details of the polarization response of SHG NCs can be found in SI section 1 and Figure S1. Figure 1b shows the SHG emission from an individual BTO NC, marked as "1" in Figure 1a, with respect to the polarization angle.

The concept of the SHaSM is depicted in Figure 1c−f. Assuming that a ring consists of 12 BTO NCs shown in Figure 1f, single-molecule imaging of each BTO NC was realized *via* a conventional second harmonic imaging microscopy (columns 1 and 2 in Figure 1d). Temporal images are achieved by controlling the excitation polarization *via* a half-waveplate (column 2 in Figure 1d). Since the BTO NCs were stochastically dispersed, the second-order nonlinear susceptibility tensors of the BTO NCs randomly orient in the 3D space. Therefore, BTO NCs randomly emit a SHG signal with high efficiency under the excitation of a linearly polarized light. For each SHIM image, a point spread function (PSF) (eq 1) was used to localize the coordinates of the BTO NC.[36]

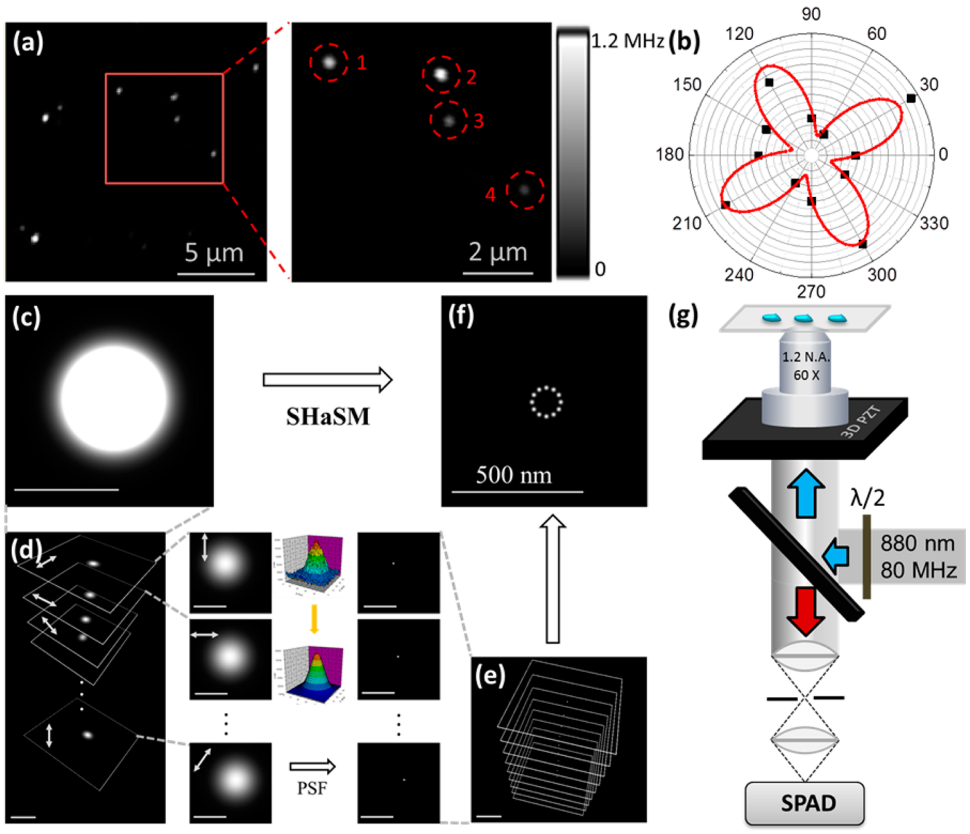

Figure 1. Characterization of optical properties of BTO probes and illustration of the concept of SHaSM. (a) SHIM image of individual unfunctionalized BTO NCs on the coverslip. (b) Tunable SHG emission from individual BTO NC (marked as "1" in (a)) at consecutive polarization angles (0 to 360°); black spots are experimental measurements, and the red line is the fitting. (c−f) Concept of SHaSM. For an aggregate of BTO NCs forming a ring shape (f), in a conventional SHIM image, only one spot is visualized (c); temporal images are obtained in conventional SHIM by the control of excitation polarization *via* a half-waveplate (d); diffraction-limited spots of SHG signal are fitted by point spread function to obtain localizations of each spot (d). Super-resolution image is obtained by overlapping the coordinates of the temporal images (e,f). (g) Layout of the SHaSM instrumention.

$$P(x,y) = I_0 + A\exp\left[-\frac{1}{2}\left[\left(\frac{(x-x_0)}{s_x}\right)^2 + \left(\frac{(y-y_0)}{s_y}\right)^2\right]\right] \quad (1)$$

where $P(x,y)$ is the 2D PSF on the xy plane, I_0 is the background intensity, A is the amplitude of the spot, x_0 and y_0 are coordinates of localization, and s_x and s_y are width of the PSF in x and y directions, respectively. By fitting, the coordinates can be localized with the standard deviation smaller than 1 nm (column 4 in Figure 1d).[27] Super-resolution is therefore realized by superimposing all of the fitted coordinates of each BTO NC into one image (Figure 1e,f). Details of the algorithm can be found in SI section 2. The BTO ring, which cannot be resolved by scanning microscopy (Figure 1c), is identified by the SHaSM as shown in Figure 1f. Figure 1g shows the basic layout of SHaSM, which was constructed on the bench of a multiphoton microscope. A Chameleon Ultra Ti-Sapphire tunable laser (Coherent Inc., CA.) operating at 880 nm with 140 fs pulse and 80 MHz repetition frequency was used as the excitation source. The laser beam was modulated *via* a half-waveplate (10RP52-2, Newport) mounted on a motorized rotation stage (PRM1Z8, Thorlabs) before being delivered onto the sample by a water-immersion objective (60×/1.20, Olympus). The SHG signal was collected using the same objective and further filtered by a short-pass filter and a band-pass filter (460-50, Chroma) before reaching the single-photon avalanche photodiodes (SPAD) (SPCM-AQR-14, PerkinElmer Inc.).

Figure 2 shows the proof-of-concept experiment of the SHaSM, which is validated by visualizing the BTO NCs beyond the diffraction limit. BTO NCs shown in Figure 1b and Figure 2b were processed by the SHaSM and led to a super-resolution image, as depicted in Figure 2e. For better comparison, BTO NC marked as spot "1" was elaborated with SHIM and SHaSM images shown in Figure 2a,d, respectively. In addition, the BTO NC marked as spot "2" was zoomed in, as shown in Figure 2c,f. Different from spot "1", spot "2" has a much more complicated emission profile with respect to the incident polarization (SI Figure S2). This indicates that more than one BTO NC exists in the spot, which is confirmed by the SHaSM. Only a single BTO NC was

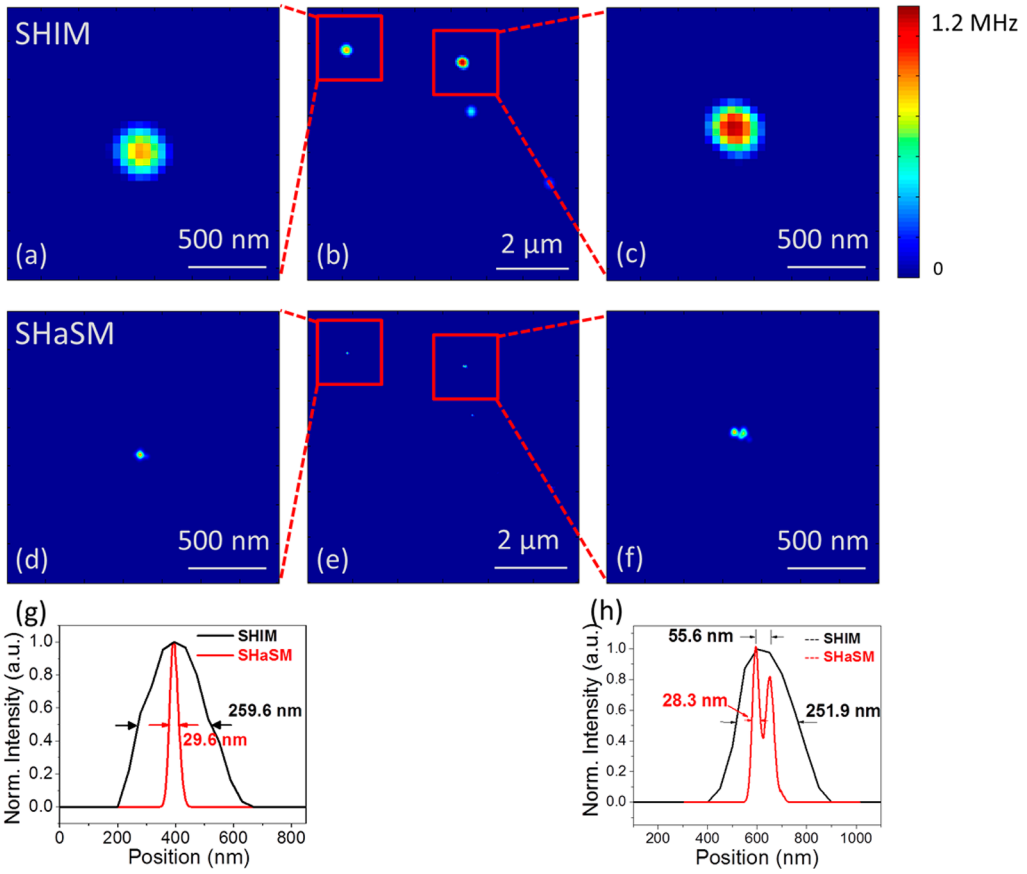

Figure 2. Proof-of-concept super-resolution image of BTO NCs on a coverslip *via* the SHaSM. (a–c) Diffraction-limited SHIM images of BTO NCs on the coverslip; (a,c) zoomed-in images of BTO NCs marked as spots "1" and "2", respectively. (d–f) Nanoscale images beyond the diffraction limit of BTO NCs corresponding to (a–c). (g,h) Cross-section distribution of BTO NCs *via* SHIM (black) and the SHaSM (red). (g) Spot "1" and (h) Spot "2".

noted in spot "1" (Figure 2d), while two BTO NCs were observed in spot "2" (Figure 2f). To characterize the SHaSM, the cross-sectional distributions of SHIM and SHaSM images are plotted in Figure 2g,h for spot "1" and "2", respectively. The full width at half-maximum (fwhm) of spots in Figure 2a,c is ~250 nm, the spatial resolution of the SHIM. In contrast, fwhm values of spots in SHaSM images are around 28 nm, about 9 times smaller than the diffraction limit. In addition, in Figure 2h, we show that the SHaSM can identify two adjacent BTO NCs with a center-to-center distance of 55.6 nm, which is the closest distance between two adjacent BTO NCs, as the first demonstration of second harmonic super-resolution imaging. Here we define the fwhm of a single spot (28.3 nm) as the localization precision of the SHaSM and 55.6 nm as the spatial resolution of the SHaSM. It should be noted here that in the SHaSM we localized the centroid of the 80 nm crystal, with the localization accuracy of ~28 nm. This value is smaller than the size of the nanocrystal and allows us to distinguish two adjunct particles with the size of ~80 nm. The estimated localization precision stems from the large-diameter BTO NCs since the SHG signal is evaluated based on the assembly of all of the unit cells in a single particle. This localization resolution can be improved to a few nanometers if smaller NCs are used, making the SHaSM a competitive super-resolution imaging approach with similar resolution as other super-localization/resolution microscopy techniques based on fluorophores or quantum dots.[3−5,37]

Given the evidence that the SHaSM can resolve single BTO NCs with a lateral resolution of ~28 nm, we developed oligonucleotide probes with BTO NCs as "reporters" for the detection of single mRNA beyond the diffraction limit. BTO NCs were initially chemically modified following the protocol in Figure 3a. Then thiol-terminated oligonucleotides were attached onto the surface-modified BTO NCs to form a BTO "monomer" (Materials and Methods). We proposed a "dimer" configuration of BTO NCs for mRNA detection instead of linearly hybridizing BTO "monomers" due to the detection specificity. Two different oligonucleotide probes (probe strand (PS) and capture strand (CS)), which possess adjacent complementary sequences to the targeting mRNA, are conjugated to the BTO NCs. The 3′-thiolated end of PS and 5′-thiolated end of CS are connected to the surface of BTO NCs to form the two types of BTO "monomers" (BTO_PS and BTO_CS). Finally, a BTO dimer can be formed upon hybridization of the mRNA (Figure 3b,d). In SHaSM, the dimer can be

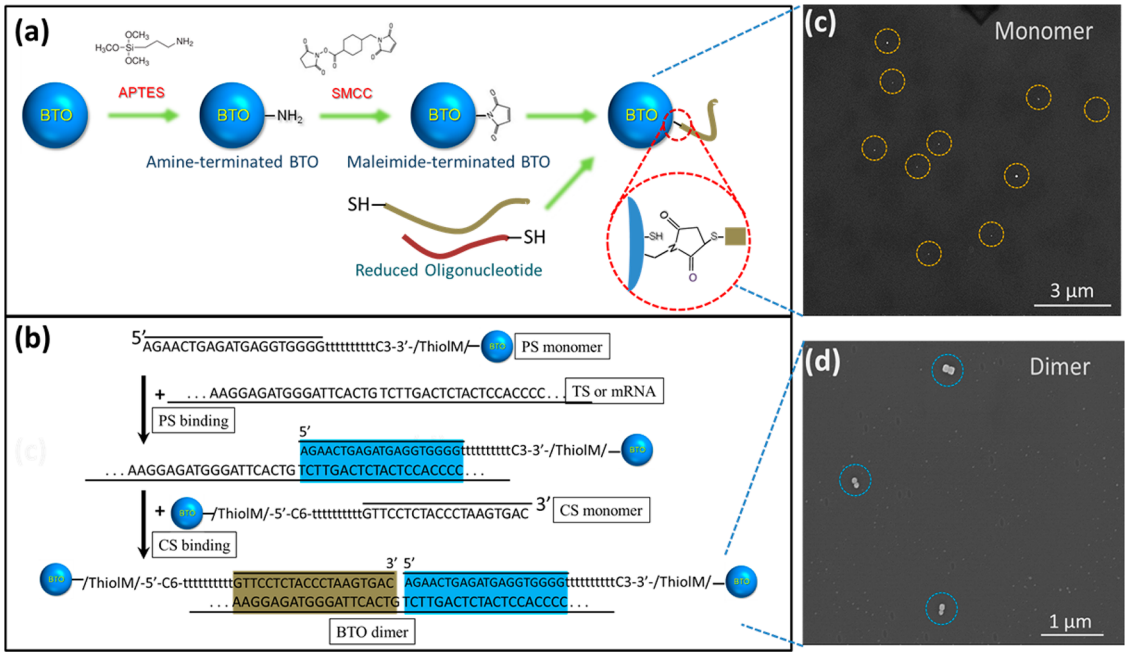

Figure 3. (a) Schematic of biofunctionalization of BTO probes used for mRNA detection. This includes sequential attachment of functional amino groups, maleimide derivatives, and oligonucleotide conjugation *via* highly reactive thiol-maleimide specificity. (b) Diagram of the hybridization of BTO dimers. SEM images of (c) BTO monomers and (d) dimers.

easily and visually seen from the images and differentiated from the background of individual NCs.

Before intracellular mRNA detection *via* the SHaSM approach, we prevalidated the hybridization of monomers to oligonucleotide sequences corresponding to a complementary mRNA sequence by *in vitro* experiments. A single-strand DNA (target strand, TS typically ~40 bps, depicting a target mRNA or miRNA) is targeted by a complementary PS (~20 bps) bearing a BTO particle and a CS (~20 bps) bearing a BTO particle consecutively to form a dimer upon hybridization. To illustrate the concept, BTO−PS and BTO−CS monomers were mixed with the solution of the TS (1:1:0.5) to result in a dimer configuration (BTO dimer) (Materials and Methods). Figure 3c,d shows scanning electron microscopy (SEM) images of BTO monomers and dimers spin-coated on the coverslip; individually distributed BTO monomers and dimers could be observed.

The *in vitro* calibration was performed to validate the SHaSM in differentiating BTO dimers from BTO monomers and for quantification. Mixture of BTO monomers and dimers in a 3:1 ratio were evaluated by SHaSM and further by SEM as the control. Figure 4a,b shows the SHIM image and SHaSM image of the mixture, respectively. The criterion for selecting a BTO dimer was based on the center-to-center distance between two monomers bearing the PS and CS hybridized to TS with a predefined interparticle spacing. Details of the algorithm used to detect and quantify BTO dimers are described in SI section 4. Distributions of BTO monomers and dimers separated from Figure 4b are shown in Figure 4c,d, respectively, and the zoomed SHIM and SHaSM images of BTO monomers and dimers are shown in Figure 4e−h. Results of the distance calculation between two monomers in over 50 BTO dimers are plotted in Figure 4i,j. Our analysis shows that the BTO dimers have an optimal interparticle distance of around 80 nm with an average at 77.36 ± 2.25 nm. The broad range of the interparticle distance of BTO dimers originates from two aspects; one is the size distribution of the BTO NCs, and the other is the geometry of the target strand (or mRNA).[38] As a control, the dimer distance measured by SEM has a similar distribution as measured by SHaSM (Figure 4i); *t* test shows excellent agreement (*p* value is 0.31). In addition, BTO dimers were also quantified by SHaSM. Figure 4k compares the measured percentage of BTO dimers in a mixture of monomer and dimer by SHaSM (left) and SEM (right). In Figure 4k, left tilted is for the mixture with a dimer/monomer ratio of 3:1 and right tilted is for a ratio of 1:0. Our study shows that the results from two different evaluations compare well and are in good agreement. It should also be noted that in the *in vitro* quantification, the percentage of measured BTO dimers did not agree well with the designed ratio; this is because, in the *in vitro* hybridization, the yield of BTO dimers was not 100% and excess BTO monomers were not isolated from dimers. However, for detection in cells, the complementary oligonucleotide probes are expected to bind to the targeting mRNA and the nonspecific BTO monomers are washed away. Overall, Figure 4i−k successfully suggests that the SHaSM can be applied to detect and quantify BTO dimers with high accuracy.

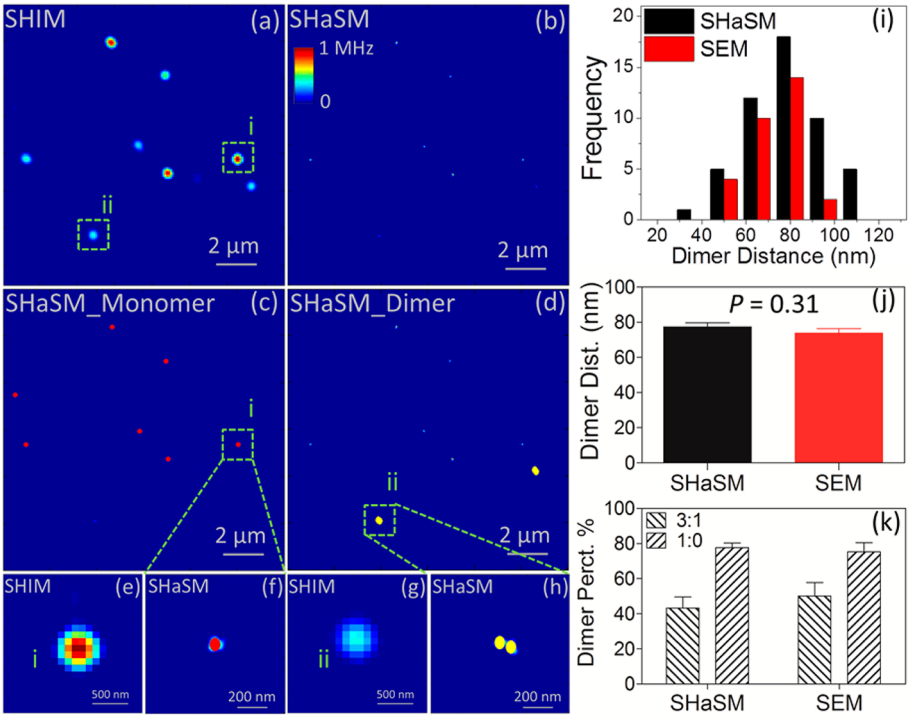

Figure 4. *In vitro* **calibration of BTO dimers by SHaSM and SEM. (a) SHIM and (b) SHaSM images of mixed BTO monomers and dimers (3:1 ratio) on the coverslip. Map of (c) BTO monomers (red dots) and (d) BTO dimers (yellow dots) differentiated by the SHaSM. (e) SHIM and (f) SHaSM images of BTO monomers marked as "i" in (a) and (c) zoomed 15 times. (g) SHIM and (h) SHaSM images of BTO dimers marked as "ii" in (a) and (d) zoomed by 15 times. (i) Histogram of the dimer distance (center-to-center distance of BTO NCs) measured by SHaSM (black) and SEM (red). (j) Statistics of the dimer distance characterized by SHaSM (black) and SEM (red); inset shows the *p* value by *t* test. (k) Percentage of dimers measured by the SHaSM and SEM in a mixture of BTO monomers and dimers in ratios of 3:1 and 1:0.**

Motivated by the capability of SHaSM to detect single BTO dimers *in vitro*, we utilized our concepts and methodology to quantify mRNA corresponding to the human epidermal growth factor receptor 2 (Her2) at the single-cell level. It is known that the overexpression of the Her2 gene is associated with the tumorigenesis of 15−20% of invasive breast cancers and can be targeted by antibody-based therapies (*e.g.*, Herceptin), whereas Her2-negative tumors require other therapeutic alternatives. The expression levels of Her2 mRNA have been used as predictive markers for diagnosis or in therapeutics for malignant tumors.[39] Our proposed approach will provide quantitative information on the transcripts at single-copy sensitivity in single cells. For the intracellular mRNA hybridization, briefly the two types of BTO monomers (BTO_CS, BTO_PS) when incubated with a target (*in vitro* or in fixed single cells) will hybridize to form a dimer configuration; details of the experimental procedure are provided in the Materials and Methods section. The selection of cell lines is based on the estimated expression level of Her2 mRNAs; it is been reported that Her2 mRNA is overexpressed in SK-BR-3 cells, moderately expressed in MCF-7 cells, and rarely expressed in HeLa cells. These cell lines were used as model systems to test the technology.

Figure 5 shows the expression of Her2 mRNA in SK-BR-3 cells (Figure 5a−c), MCF-7 cells (Figure 5d−f), and HeLa cells (Figure 5g−i). Panels a, d, and g in Figure 5 are the two-photon autofluorescence images that use 780 nm for excitation and 570−650 nm for emission; panels b, e, and h are SHG channel, and c, f, and i are merged images from both channels. For the two-photon and SHG microscopy, the laser power was set at 0.21 mW, resulting in an average intensity of 49.5 KW/cm^2 as well as a peak intensity of 5.96 GW/cm^2 at the focus, which is within the safety threshold for biological imaging.[40] Results clearly show that Her2 mRNA is overexpressed in SK-BR-3 cells and expressed in very low levels in MCF-7 and rarely in HeLa cells. By comparing the fluorescence channel and SHG channel, it can be concluded that all of the mRNAs exist in the cytoplasm of the cell lines, as expected. Details of binding specificity are provided in SI Figures S5−S7. Although a minimum nonspecific binding was noted, our protocols show that all the free BTO NCs (or monomers) are washed away. In the following sections, we detail the quantification of Her2 mRNA in SK-BR-3 cells as an example to evaluate the distribution of mRNAs and the capabilities of the SHaSM.

Figure 5j shows the zoomed SHIM image of BTO NCs in SK-BR-3 cells marked in Figure 5c, and the corresponding SHaSM image is shown in Figure 5k. The algorithm for dimer differentiation was employed to quantify BTO dimers. Briefly, all BTO NCs were initially

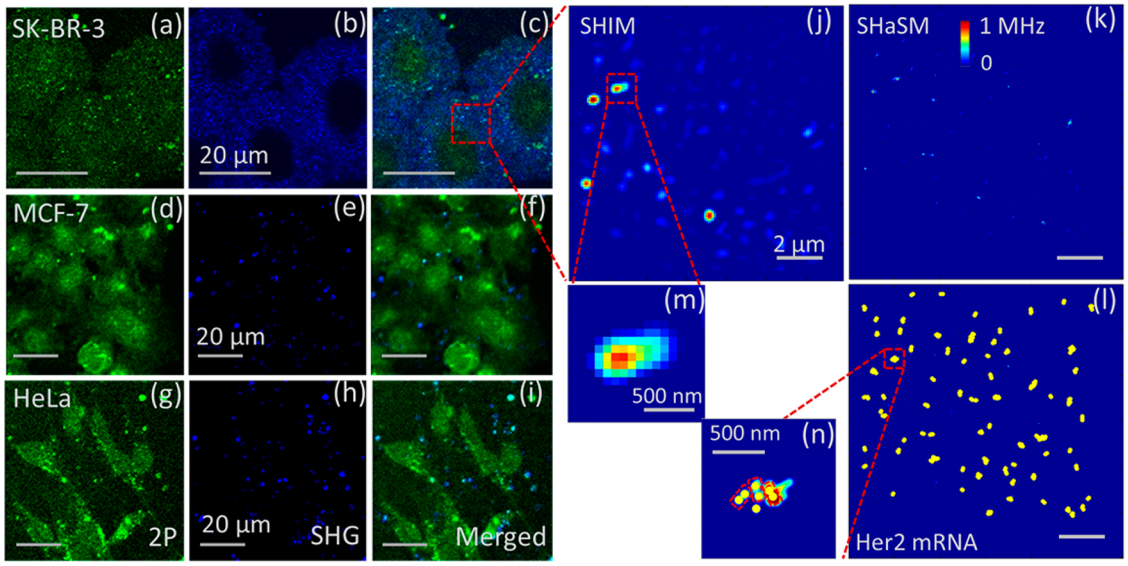

Figure 5. Detection of Her2 mRNA at single-cell resolution in three different cell lines using SHaSM. (a,d,g) Two-photon-excited autofluorescence from SK-BR-3, MCF-7, and HeLa cells, respectively, which were incubated with BTO_CS and BTO_PS probes; (b,e,h) corresponding SHIM images; (c,f,i) merged image of 2P channel and SHG channel. (j) Zoomed SHIM image of SK-BR-3 cells incubated with BTO_CS and BTO_PS probes marked in (c). (k) SHaSM image corresponding to (j). (l) Mapping of Her2 transcripts by localization of BTO dimers. (m) Zoomed-in single spot in the SHIM image. (n) Zoomed SHaSM image corresponding to (m). Scale bars: (a−i) 20 μm, (j−l) 2 μm, (m) 500 nm, (n) 500 nm.

identified as red dots in SI Figure S8; later, any two closest BTO NCs with the center-to-center distance smaller than the threshold were selected as BTO dimers, which are noted as yellow dots in Figure 5l. A BTO dimer represents a single Her2 mRNA. From the magnified image of a single bright spot in the SHIM image (Figure 5m), three mRNAs can be identified from the SHaSM image, shown as red circles highlighted in Figure 5n. However, from the SHIM image, only one mRNA was noted. Here we should point out that the aggregate of multiple mRNAs is not the polycrystalline aggregate of BTO NCs, whose polarization responses are significantly different from that of single NCs.[33,34] In our experiments, several treatment steps were performed to avoid polycrystalline aggregates. First, the surface of BTO NCs was chemically modified to ensure monodispersibility of NCs in solution, minimizing the possibility of aggregation. Second, the chemical groups ($-NH_2$, $-SH$) on the surface of BTO NCs further prevent the formation of polycrystalline structures possibly due to aggregation. Last, the spherical shape of BTO NCs minimizes the interface contribution from the SHG emission.[8] Thus, emission from a single BTO NC is not affected and is specific compared to BTO NCs in an aggregated form possibly due to the targeting and localization of multiple mRNAs.

Expression levels of Her2 mRNA were counted by the number of BTO dimers. SHaSM imaging of the whole cell can provide the quantity of transcripts, as shown in Table 1. The average number of Her2 mRNA in SK-BR-3 cells measured by SHaSM was estimated to be 595 ± 79.1 per cell. As a comparison, the expression measured by the conventional microscopy was 282 ± 54.3 per cell,

TABLE 1. Quantification of Her2 mRNA in Different Cell Lines

	Her2_SHaSM	Her2_SHIM	FISH
SK-BR-3	595 ± 79.1	282 ± 14.3	353 ± 117
MCF-7	38.9 ± 8.26	153.1 ± 11.9	13.5 ± 4.9
HeLa	1.5 ± 2.8	3.4 ± 5.8	5 ± 2.9

which is more than two times lower than that quantified by SHaSM. The discrepancy exists because SHaSM has the ability to resolve multiple mRNAs in a diffraction-limited spot which otherwise is not possible by conventional microscopy. The magnified SHaSM images demonstrate that it is possible to locate more than one mRNA in a diffraction-limited spot should these exist.

Quantification of Her2 mRNA in MCF-7 cells and HeLa cells was also performed *via* the SHaSM, and the results are provided in Table 1. Our analysis shows that the average number of Her2 mRNA quantified by the SHaSM is 38.9 ± 8.26 per cell in MCF-7 and 1.5 ± 2.8 per cell in HeLa cells, which agrees well with the past values.[41,42] However, from the SHIM images, the value noted was 153.1 ± 31.9 per cell in MCF-7 and 3.4 ± 5.8 per cell in HeLa. We are of the opinion that the discrepancy mainly stems from the background of nonspecific BTO monomers, which may bind to the active sites in the cell cytoplasm. Similar defects have also been reported for the FISH technique.[22] The SHaSM has the capability to exclude the interference from nonspecifically bound BTO monomers, and consequently, unless the Her2 mRNA is targeted by two BTO monomers, to result in a dimer formation, the

monomers will not be counted. From Table 1, it is our opinion that, in the conventional diffraction-limited mRNA quantification approach, the mRNA number is overestimated in cell lines with moderate or rare expression due to the nonspecifically bound probes, while the mRNA number is underestimated in overexpressing cell lines because of the inability to resolve several targets in one spot.

To validate our SHG probes and detection strategy, FISH experiments were performed along with conventional qPCR to compare the expression level of Her2 mRNA in the above cell lines. Results from qPCR show that the expression level of Her2 mRNA in the SK-BR-3 cell line is much higher than that observed in MCF-7 and HeLa cell lines (SI Figure S9); in addition, immunostaining for the Her2 protein on the cell membrane also indirectly suggests that Her2 mRNA is overexpressed in SK-BR-3 cells (SI Figure S11). Furthermore, quantitative FISH images, as shown in SI Figure S10 and Table 1, indicate that the average number of Her2 mRNA in SK-BR-3, MCF-7, and HeLa cell lines is comparable to the results detected by the SHaSM and is close to the theoretical estimates reported by other works *via* FISH.[41,42]

Overall, the SHaSM approach offers significant accuracy and specificity compared to the conventional diffraction-limited detection methods for transcript quantification in single cells, especially for cells with highly expressed mRNA transcripts. The theoretical maximum number of SHG probes detected by the SHaSM is about 8−10 in each diffraction-limited spot (~250 nm in diameter), resulting in a probing range of approximately 40−50/μm^2, suggesting the theoretical quantification limit of 10 000−15 000 transcripts per cell. Furthermore, this quantification limit can be extended with a polarization analyzer (typically inserted before the detector) to improve the contrast between different polarization angles. By SHaSM, we will have the ability to "see" individual BTO NCs and thus "visualize" single mRNA, which is almost impossible by other super-resolution microscopy techniques due to the optical constraints posed by fluorescent probes. It is worth noting that in our design the SHG probes have minimal requirements on the length of the targeting mRNA and hence are suitable for the detection of any single mRNA with a short sequence length; in addition, only two BTO NCs (BTO_CS and BTO_PS) are required to target each transcript to detect and quantify Her2 mRNA; this design is also possible to implement *via* plasmonic nanoparticles[43] and hyper-spectral super-resolution approach.[44,45]

The localization precision and lateral resolution of SHaSM in our experiment was estimated to be ~28 and ~56 nm, but in theory, these two values can reach single digits. In a typical scanning image with a 200 μs dwell time, N = ~2000 photons can be collected from a single BTO NC to yield the theoretical spatial resolution as $1/\sqrt{N}$.[46] However, in our experiment, the lateral resolution is restricted due to the volume of the BTO NCs. In addition, the SHaSM also has the potential for rapid imaging. By optimizing the photons collected in each pixel, we can improve the scanning speed of the SHIM image to 500 frames per second, but still with high SNR ratio (>100). Even if every 50th SHIM image is processed to obtain a super-resolution map by the second harmonic generation process, at least 10 frames of the super-resolution SHG image can be realized per second, which is sufficient to monitor the dynamics of intricate intracellular behavior compared to nonfluorescent approaches.[43,47−49] Furthermore, we anticipate that the imaging speed can reach video rates if scan-free instrumentation is used in the future.[14]

CONCLUSIONS

To summarize, we present a SHaSM platform by taking advantage of SHG signals from BTO NCs to demonstrate single-molecule sensitivity at a resolution of a few tens of nanometers. *In vitro* experiments consistently demonstrate the capability of SHaSM to differentiate two individual BTO NCs separated by a center-to-center distance of 55.6 nm with a localization resolution of ~28 nm. The BTO NCs were functionalized with complementary oligonucleotide sequences to hybridize with target-specific mRNA for visualization at super-resolution scale and quantification at single-copy sensitivity. The SHaSM approach conceptualized was utilized to not only visualize the localization patterns but also to quantify the expression levels of individual Her2 mRNA in fixed SK-BR-3, MCF-7, and HeLa cell lines, suggesting that the number of copies of Her2 mRNA in the respective cell lines were 595 ± 79.1, 38.9 ± 8.26, and 1.5 ± 2.8, respectively, and was in good agreement with the theoretical calculations and validated with FISH and qPCR experiments. We expect the quantification technology will allow scientists to "see" individual mRNA transcripts inside a single cell and to elucidate gene expression patterns in specific phenotypes at different stages of tissue differentiation. Such knowledge will be paramount for human health as defects in transcription adversely affect normal growth and differentiation, which will impact both clinical diagnostics and basic biology.

MATERIALS AND METHODS

Chemicals and Reagents. Thiol-modified and simple DNA oligonucleotides were obtained from IDT (Coralville, IA). The oligonucleotides were of highest quality, purified either using HPLC or from PAGE gels. Succinimidyl-4-(*N*-maleimidomethyl)-cyclohexane-1-carboxylate (SMCC) was purchased from Pierce

(Rockford, IL). Tris(2-carboxyethyl)phosphine hydrochloride (TCEP), Tween-20, trisodium citrate dehydrate, ethylenediaminetetraacetic acid disodium salt (EDTA), (3-aminopropyl)-triethoxysilane (APTES), dimethyl sulfoxide (DMSO), and 0.2 μm pore PVDF filter membrane were obtained from Sigma-Aldrich (St. Louis, MO). Common reagents used in this study were of standard research quality, purchased from Purdue University chemical stores.

Chemical Functionalization of BTO Probes. In this work, we select BTO NCs as SHG probes due to their nontoxicity and biocompatibility. Hexagonal BTO NCs were gifted by Prof. Paul Bowen (Swiss Federal Institute of Technology, Lausanne, Switzerland).[50] Dried BTO NC powder was first dissolved in water in a ratio of 10 mg to 100 mL and sonicated for 20 min to obtain monodispersed NCs and then filtered by a 0.2 μm pore filter membrane three times to exclude aggregates. The prepared BTO NCs were immersed in 1 M of sulfuric acid for 10 min to remove the surface barium ions followed by discarding supernatant after centrifugation (6500 rpm, 20 min). The surface-activated BTO then reacted with 0.1% APTES dissolved in anhydrous ethanol at 70 °C for 2 h to functionalize the surfaces as amine. After the unreacted APTES was removed by centrifugation, the NCs were mixed with 2 mM of SMCC dissolved in DMSO and kept at room temperature for 1 h. Free SMCC was removed by centrifugation.

BTO−Oligonucleotide Hybridization. Three different oligonucleotide strands (TS, PS, and CS) were designed using NCBI Blast, and these oligonucleotides were purchased from IDT-DNA, Inc. (Coralville, IA). The 3′-thiolated end (probe strand) and 5′-thiolated end (capture strand) oligonucleotides were used for the conjugation with BTO NCs; each oligonucleotide is made up of 10 base pairs of linkers along with 20 base pairs of complementary sequences. In addition, a complementary oligonucleotide target strand for the probe strand and capture strand was also used here to form an *in vitro* dimer structure as a control.

probe strand (PS): 5′-AGAACTGAGATGAGGTGGGGttttttttttt-C3-3′-/ThiolM/

capture strand (CS): /ThiolM/-5′-C6-ttttttttttGTTCCTCTACC-CTAAGTGAC-3′

target strand (TS): AAGGAGATGGGATTCACTGTCTTGACT-CTACTCCACCCC

We adopted the protocol of gold nanoparticle hybridization with oligonucleotides previously used in our group with minor modifications.[51,52] DNA oligonucleotides were first dissolved in 10:1 TE (Tris-EDTA) buffer to make a 100 μM solution; the disulfide bond of thiolated DNA oligonucleotide probe was then broken using a 10 mM solution of TCEP (at room temperature, shaking for 10−15 min). These reduced thiolated DNA strands (1 μM) were then reacted with 1 mL of the functionalized (thiol-reactive) BTO NC solution to obtain 1 mL of DNA−BTO conjugate solution (at ∼60 °C for 30 min to 1 h). The residual surfaces were finally blocked with 10 mM mercaptoethanol. Next, the solution was washed with nanopure water (18.2 mΩ, Milli-Q, Inc.). Finally, the resulting DNA−BTO probes were washed three times with 0.3 M PBS to remove unbound oligosequences. After successful conjugation, all prepared probes were stored at 4 °C until further use.

For control experiments, BTO dimers *in vitro*, constituting probe-strand-conjugated BTO NCs and capture-strand-conjugated BTO NCs, were mixed in equal proportions, and then the target strand was added in lower concentration than the conjugated BTO NCs (2:1); the mixture was kept at a temperature of 60 °C, which was lower than the melting point of the DNA hybridization. Electron microscopy (Figure 3) and dynamic light scattering (SI section 1) experiments were used to characterize the function and conjugation of BTO probes.

Cell Culture and Incubation with BTO Probes. The standard culture media used for SK-BR-3, MCF-7, and HeLa was Dulbecco's modified Eagle's medium supplemented with 10% fetal bovine serum. Cells were seeded onto the sterilized no. 1 coverslips (VWR International, Batavia, IL) inside a 6-well plate with culture medium and maintained at 37 °C in an atmosphere of 5% CO_2; after reaching 80% confluence, cells were rinsed by PBS three times and then fixed by 4% paraformaldehyde for 15 min; after being washed by PBS three times, cells were permeabilized by 0.1% Triton-X for 2 h; in the end, cells were washed by PBS. For mRNA detection, fixed cells were incubated with functionalized BTO−oligonucleotide probes (probe strand and capture strand at the same concentration) at room temperature overnight in the PBS and then washed with gentle shaking and stored in PBS at 4 °C for SHaSM imaging.

Conflict of Interest: The authors declare no competing financial interest.

Acknowledgment. Research was possible by grants from NSF (Award No. 1249315), the Showalter Trust Grant, the W.M. Keck Foundation, the SIRG fellowship from the Purdue Center for Cancer Research (NIH-NCI P30 CA023168), the CTSI NIH-NCI grant, and the Ismail Travel Grant from Purdue University. We thank Jingwen Yan (Indiana University), Jiji Chen (Howard Hughes Medical Institute) for programming assistance, and Basudev Chowdhury, Zhongwu Zhou, and Nur Damayanti for providing the SK-BR-3, MCF-7, and HeLa cell lines. Ulhas Kadam is acknowledged for help in oligonucleotide−nanocrystal conjugation. We also thank Prof. Paul Bowen (EPFL, Switzerland) for providing the BTO NCs. Nathaniel Kinsey is acknowledged for edits and general comments on the manuscript.

Supporting Information Available: Additional information and figures. This material is available free of charge *via* the Internet at http://pubs.acs.org.

REFERENCES AND NOTES

1. Abbe, E. Beitrage zur Theorie des Mikroskops und der Mikroskopischen Wahrnehmung. *Arch. Mikrosk. Anat.* **1873**, *9*, 413–420.
2. Hell, S. W. Far-Field Optical Nanoscopy. *Science* **2007**, *316*, 1153–1158.
3. Betzig, E.; Patterson, G. H.; Sougrat, R.; Lindwasser, O. W.; Olenych, S.; Bonifacino, J. S.; Davidson, M. W.; Lippincott-Schwartz, J.; Hess, H. F. Imaging Intracellular Fluorescent Proteins at Nanometer Resolution. *Science* **2006**, *313*, 1642–1645.
4. Hess, S. T.; Girirajan, T. P. K.; Mason, M. D. Ultra-high Resolution Imaging by Fluorescence Photoactivation Localization Microscopy. *Biophys. J.* **2006**, *91*, 4258–4272.
5. Rust, M. J.; Bates, M.; Zhuang, X. Sub-diffraction-Limit Imaging by Stochastic Optical Reconstruction Microscopy (STORM). *Nat. Methods* **2006**, *3*, 793–795.
6. Patterson, G.; Davidson, M.; Manley, S.; Lippincott-Schewartz, J. Superresolution Imaging Using Single Molecule Localization. *Annu. Rev. Phys. Chem.* **2010**, *61*, 345–367.
7. Dempsey, G. T.; Vaughan, J. C.; Chen, K. H.; Bates, M.; Zhuang, X. Evaluation of Fluorophores for Optimal Performance in Localization-Based Super-resolution Imaging. *Nat. Methods* **2011**, *8*, 1207–1036.
8. Boyd, R. W. *Nonlinear Optics*; Academic: San Diego, CA, 2003.
9. Pantazis, P.; Maloney, J.; Wu, D.; Fraser, S. Second Harmonic Generating (SHG) Nanoprobes for *In Vivo* Imaging. *Proc. Natl. Acad. Sci. U.S.A.* **2010**, *107*, 14535–14540.
10. Staedler, D.; Magouroux, T.; Hadji, R.; Joulaud, C.; Extermann, J.; Schwung, S.; Passemard, S.; Kasparian, C.; Clarke, G.; Gerrmann, M.; *et al.* Harmonic Nanocrystals for Biolabeling: A Survey of Optical Properties and Biocompatibility. *ACS Nano* **2012**, *6*, 2542–2549.
11. Dempsey, W. P.; Fraser, S. E.; Pantazis, P. SHG Nanoprobes: Advancing Harmonic Imaging in Biology. *Bioessays* **2012**, *34*, 351–360.
12. Bonacina, L. Nonlinear Nanomedecine: Harmonic Nanoparticles toward Targeted Diagnosis and Therapy. *Mol. Pharmaceutics* **2013**, *10*, 783–792.
13. Le, X. L.; Zhou, C.; Slablab, A.; Chauvat, D.; Tard, C.; Perruchas, S.; Gacoin, T.; Villeval, P.; Roch, J. F. Photostable Second-Harmonic Generation from a Single $KTiOPO_4$ Nanocrystal for Nonlinear Microscopy. *Small* **2008**, *4*, 1332–1336.
14. Hsieh, C. L.; Grange, R.; Pu, Y.; Psaltis, D. Bioconjugation of Barium Titanate Nanocrystals with Immunoglobulin G

Antibody for Second Harmonic Radiation Imaging Probes. *Biomaterials* **2010**, *31*, 2272–2277.
15. Grange, R.; Lanvin, T.; Hsieh, C.; Pu, Y.; Psaltis, D. Imaging with Second-Harmonic Radiation Probes in Living Tissue. *Biomed. Opt. Express* **2011**, *2*, 2532–2539.
16. Geissbuehler, M.; Bonacina, l.; Shcheslavskiy, V.; Bocchio, N. L.; Geissbuehler, S.; Leutenegger, M.; Marki, I.; Wolf, J.; Lasser, T. Nonlinear Correlation Spectroscopy (NLCS). *Nano Lett.* **2012**, *12*, 1668–1672.
17. Liu, J.; Irudayaraj, J. Second Harmonic Generation Correlation Spectroscopy at Single Molecule Level. *Opt. Express* **2013**, *21*, 27063–27073.
18. Culic-Viskota, J.; Dempsey, W. P.; Fraser, S. E.; Pantazis, P. Surface Functionalization of Barium Titanate SHG Nanoprobes for *In Vivo* Imaging in Zebrafish. *Nat. Protoc.* **2012**, *7*, 1618–1633.
19. Petersen, O. W. Stem Cells in the Human Breast. *Cold Spring Harbor Perspect. Biol.* **2010**, *2*, A003160.
20. Baker, M. RNA Imaging *in Situ*. *Nat. Methods* **2012**, *9*, 787–790.
21. St. Johnston, D. Moving Messages: The Intracellular Localization of mRNA. *Nat. Rev. Mol. Cell Biol.* **2005**, *6*, 363–375.
22. Femino, A. M.; Fay, F. S.; Fogarty, K.; Singer, R. H. Visualization of Single RNA Transcripts *in Situ*. *Science* **1998**, *280*, 585–590.
23. Raj, A.; van den Bogaard, P.; Rifkin, S. A.; van Oudenaarden, A.; Tyagi, S. Imaging Individual mRNA Molecules Using Multiple Singly Labeled Probes. *Nat. Methods* **2008**, *5*, 877–879.
24. Grunwald, D.; Singer, R. H. *In Vivo* Imaging of Labelled Endogenous B-Actin mRNA during Nucleocytoplasmic Transport. *Nature* **2010**, *467*, 604–607.
25. Trcek, T.; Larson, D.; Moldon, A.; Query, C. C.; Singer, R. H. Single-Molecule mRNA Decay Measurements Reveal Promoter-Regulated mRNA Stability in Yeast. *Cell* **2011**, *147*, 1484–1497.
26. Paige, J. S.; Wu, K. Y.; Jaffrey, S. R. RNA Mimics of Green Fluorescent Protein. *Science* **2011**, *333*, 642–646.
27. Hansen, C. H.; van Oudenaarden, A. Allele-Specific Detection of Single mRNA Molecules *in Situ*. *Nat. Methods* **2013**, *10*, 869–873.
28. Mueller, F.; Senecal, A.; Tantale, K.; Marle-Nelly, H.; Ly, N.; Collin, O.; Basyuk, E.; Bertrand, E.; Darzacq, X.; Zimmer, C. Fish-Quant: Automatic Counting of Transcripts in 3D Fish Images. *Nat. Methods* **2013**, *10*, 277.
29. Bao, G.; Rhee, W. J.; Tsourkas, A. Fluorescent Probes for Live-Cell RNA Detection. *Annu. Rev. Biomed. Eng.* **2009**, *11*, 25–47.
30. Santangelo, P.; Nitin, N.; Bao, G. Nanostructured Probes for RNA Detection in Living Cells. *Annu. Biomed. Eng.* **2006**, *34*, 39–50.
31. Randolph, J.; Waggoner, A. S. Stability, Specificty and Fluorescence Brightness of Multiply-Labeled Fluorescence DNA Probes. *Nucleic Acids Res.* **1997**, *25*, 2923–2929.
32. Hsieh, C.; Pu, Y.; Grange, R.; Psaltis, D. Second Harmonic Generation from Nanocrystals under Linearly and Circularly Polarized Excitations. *Opt. Express* **2010**, *18*, 11917–11932.
33. Brasselet, S.; Floc'h, V. L.; Treussart, F.; Roch, J.; Zyss, J.; Botzung-Appert, E.; Lbanez, A. *In Situ* Diagnostics of the Crystalline Nature of Single Organic Nanocrystals by Nonlinear Microscopy. *Phys. Rev. Lett.* **2004**, *92*, 207401.
34. Bonacina, L.; Mugnier, Y.; Courvoisier, F.; Le Dantec, R.; Extermann, J.; Lambert, Y.; Boutou, V.; Galez, C.; Wolf, J.-P. Polar $Fe(IO_3)_3$ Nanocrystals as Local Probes for Nonlinear Microscopy. *Appl. Phys. B: Laser Opt.* **2007**, *87*, 399–403.
35. Mayer, L.; Slablab, A.; Dantelle, G.; Jacques, V.; Lepagnol-Bestel, A.-M.; Perruchas, S.; Spinicelli, P.; Thomas, A.; Chauvat, D.; Simonneau, M.; *et al.* Single KTP Nanocrystals as Second-Harmonic Generation Biolabels in Cortical Neurons. *Nanoscale* **2013**, *5*, 8466–8471.
36. Yildiz, A. E.; Forkey, J. N.; McKinney, S. A.; Ha, T.; Goldman, Y. E.; Selvin, P. R. Myosin V Walks Hand-over-Hand: Single Fluorophore Imaging with 1.5-nm Localization. *Science* **2003**, *300*, 2061–2065.
37. Wang, Y.; Fruhwirth, G.; Cai, E.; Ng, T.; Selvin, P. R. 3D Super-resolution Imaging with Blinking Quantum Dots. *Nano Lett.* **2013**, *13*, 5233–5241.
38. Sato, K.; Hamada, M.; Asai, K.; Mituyama, T. CENTROIDFOLD: A Web Server for RNA Secondary Structure Prediction. *Nucleic Acids Res.* **2009**, *37*, W277–W280.
39. Mitri, Z.; Constantine, T.; O'Regan, R. The Her2 Receptor in Breast Cancer: Pathophysiology, Clinical Use, and New Advances in Therapy. *Chemother. Res. Pract.* **2012**, *2012*, 743193.
40. Konig, K. Cell Damage during Multi-photon Microscopy. In *Handbook of Biological Confocal Microscopy*; Pawley, J. B., Ed.; Springer: Berlin, 2006; pp 680−689.
41. Orjalo, A., Jr.; Johansson, H. E.; Ruth, J. L. Stellaris Fluorescence *in Situ* Hybridization (FISH) Probes: A Powerful Tool for mRNA Detection. *Nat. Methods* **2011**, 10.1038/nmeth.f.349.
42. Affymetrix. *Quantigene Assays for Cancer and Disease*, 2013.
43. Lee, K. C.; Cui, Y.; Lee, L. P.; Irudayaraj, J. Quantitative Imaging of Single mRNA Splice Variants in Living Cells. *Nat. Nanotechnol.* **2014**, *9*, 474–480.
44. Huang, T.; Xu, X. N. Multicolored Nanometer-Resolution Mapping of Single Protein−Ligand Binding Complexes Using Far-Field Photostable Optical Nanoscopy (Photon). *Nanoscale* **2011**, *3*, 3567.
45. Huang, T.; Browning, L. M.; Xu, X. N. Far-Field Photonstable Optical Nanoscopy (Photon) for Real-Time Super-Resolution Single-Molecular Imaging of Signaling Pathways of Single Live Cells. *Nanoscale* **2012**, *4*, 2797–2812.
46. Russell, E.; Thompson, D. R. Precise Nanometer Localization Analysis for Individual Fluorescent Probes. *Biophys. J.* **2002**, *82*, 2775–2783.
47. Lee, K.; Drachev, V.; Irudayaraj, J. DNA-Gold Nanoparticle Networks Grown at Cell Surface Marker Sites: Diagnostics of Cancer Stem Cells. *ACS Nano* **2011**, *5*, 2109–2117.
48. Sun, L.; Yu, C.; Irudayaraj, J. Raman Multiplexers for Alternative Gene Splicing. *Anal. Chem.* **2008**, *80*, 3342–3349.
49. Yu, C.; Nakshatri, H.; Irudayaraj, J. Identity Profiling of Cell Surface Markers by Multiplex Gold Nanorod Probes. *Nano Lett.* **2007**, *7*, 2300–2306.
50. Aimable, A.; Jongen, N.; Testino, A.; Donnet, M.; Lemaitre, J.; Hofmann, H.; Bowen, P. Precipitation of Nanosized and Nanostructured Powders: Process Intensification Using SFTR, Applied to $BaTiO_3$, $CaCO_3$ and ZnO. *Chem. Eng. Technol.* **2011**, *34*, 344–352.
51. Kadam, U.; Moeller, C. A.; Irudayaraj, J.; Schulz, B. Effect of T-DNA Insertions on mRNA Transcript Copy Numbers Upstream and Downstream of the Insertion Site in *Arabidopsis thaliana* Explored by Surface Enhanced Raman Spectroscopy. *Plant Biotechnol. J.* **2014**, *12*, 568–577.
52. Sun, L.; Irudayaraj, J. Quantitative Surface-Enhanced Raman for Gene Expression Estimation. *Biophys. J.* **2009**, *96*, 4709–4716.